Hybrid Quantum/Classical Simulations of the Vibrational Relaxation of the Amide I Mode of N-Methylacetamide in D2O Solution

ARTICLE *in* THE JOURNAL OF PHYSICAL CHEMISTRY B · MARCH 2012

Impact Factor: 3.3 · DOI: 10.1021/jp210727u · Source: PubMed

6 AUTHORS, INCLUDING:

Adolfo Bastida
University of Murcia
82 PUBLICATIONS **857** CITATIONS
SEE PROFILE

Miguel Soler
University of Udine
15 PUBLICATIONS **105** CITATIONS
SEE PROFILE

Alberto Requena
University of Murcia
138 PUBLICATIONS **1,243** CITATIONS
SEE PROFILE

Sebastian Fernandez-Alberti
National University of Quilmes
46 PUBLICATIONS **696** CITATIONS
SEE PROFILE

THE JOURNAL OF PHYSICAL CHEMISTRY B

Article

pubs.acs.org/JPCB

Hybrid Quantum/Classical Simulations of the Vibrational Relaxation of the Amide I Mode of *N*-Methylacetamide in D_2O Solution

Adolfo Bastida,*[,†] Miguel A. Soler,[†] José Zúñiga,[†] Alberto Requena,[†] Adrián Kalstein,[‡] and Sebastián Fernández-Alberti*[,‡]

[†]Departamento de Química Física, Universidad de Murcia, 30100 Murcia, Spain

[‡]Universidad Nacional de Quilmes, Roque Saenz Peña 352, B1876BXD Bernal, Argentina

ABSTRACT: Hybrid quantum/classical molecular dynamics (MD) is applied to simulate the vibrational relaxation (VR) of the amide I mode of deuterated *N*-methylacetamide (NMAD) in aqueous (D_2O) solution. A novel version of the vibrational molecular dynamics with quantum transitions (MDQT) treatment is developed in which the amide I mode is treated quantum mechanically while the remaining degrees of freedom are treated classically. The instantaneous normal modes of the initially excited NMAD molecule (INM_0) are used as internal coordinates since they provide a proper initial partition of the system in quantum and classical subsystems. The evolution in time of the energy stored in each individual normal mode is subsequently quantified using the hybrid quantum-classical instantaneous normal modes (INM_t). The identities of both the INM_0s and the INM_ts are tracked using the equilibrium normal modes (ENMs) as templates. The results extracted from the hybrid MDQT simulations show that the quantum treatment of the amide I mode accelerates the whole VR process versus pure classical simulations and gives better agreement with experiments. The relaxation of the amide I mode is found to be essentially an intramolecular vibrational redistribution (IVR) process with little contribution from the solvent, in agreement with previous theoretical and experimental studies. Two well-defined relaxation mechanisms are identified. The faster one accounts for ≈40% of the total vibrational energy that flows through the NMAD molecule and involves the participation of the lowest frequency vibrations as short-life intermediate modes. The second and slower mechanism accounts for the remaining ≈60% of the energy released and is associated to the energy flow through specific mid-range and high-frequency modes.

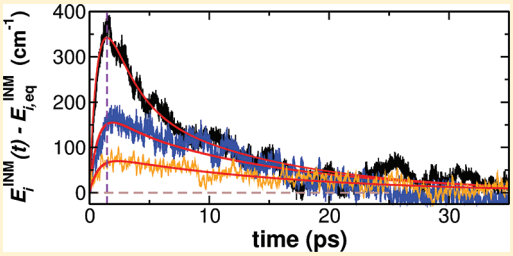

1. INTRODUCTION

Current progress in ultrafast time-resolved infrared-Raman spectroscopy[1−14] applied to the study of vibrational relaxation (VR) and intramolecular vibrational redistribution (IVR) provides unprecedented details of the transient energy content of individual vibrations of polyatomic molecules in solution, and these advances are accompanied by a number of theoretical approaches which allows different issues of the molecular origin of VR and IVR[15−31] to be successfully unraveled. In this context, compounds with peptide bonds have attracted special interest due to the fundamental role that they play in a large variety of biological processes.[32−44] The amide I mode, primarily associated with the peptide bond carbonyl stretch,[45] has been frequently probed in experiments since its strong transition dipole makes it possible to discern the spectral contributions of this mode easily.[4,46−50] In addition, the couplings of the amide I modes regularly distributed inside a protein result in an amide I band whose frequency, bandwidth, and intensity are sensitive to the topology of the hydrogen-bonded network that defines the secondary structure of the protein. This is the reason why the amide I band is widely employed in protein structural analysis. Time-domain measurements have shown that the VR rate of the amide I mode is to a certain extent insensitive to the environment, with a lifetime of the order of 1 ps for most systems studied.[4] This feature indicates that a starting detailed description of the amide I mode relaxation can be made through the study of the *N*-methylacetamide, which is the simplest molecule presenting a peptide bond, not losing sight nevertheless of the fact that relaxation of the amide I vibrations of proteins can be considerably more complicated because of the coupling of nearby amide groups.

The VR of deuterated *N*-methylacetamide (NMAD) in solution has been the subject of a wide number of both experimental[4,6,6,10,51−56] and theoretical[52,57−69] studies, which altogether have provided a qualitative picture of the main relaxation channels involved in the process. Discrepancies however in the kinetic interpretation of the vibrational energy decay and uncertainties in the values of the relaxation lifetimes of the amide I mode, as extracted from different experimental measurements,[4,54] show that an ultimate accurate description of the VR of NMAD is still pending.

Among the theoretical treatments developed to shed light on the VR of NMAD, nonequilibrium classical molecular dynamics (MD) simulations in combination with instantaneous normal modes (INMs) analysis[70−78] have been shown to provide

Received: November 8, 2011
Revised: February 2, 2012
Published: February 4, 2012

valuable information about the vibrational energy flow through the molecule following relaxation of the amide I mode.[58,67] Recent nonequilibrium MD-INM simulations of the photo excitation and subsequent VR of both the amide I mode[68] and the C−H stretching modes ($\nu_s(CH_3)$)[69] of NMAD in liquid D_2O have made it possible to track the time evolution of the excesses of vibrational energy stored in each individual INM of NMAD and compare them directly with data provided by time-resolved infrared-Raman spectroscopic measurements.[4,54,55] Despite the success of the MD-INM method in giving a confident qualitative description of the main NMAD IVR pathways, it still lacks a certain degree of quantitative accuracy since it provides relaxation rates which are several times smaller than those from experiments.[58,68,69]

Perturbation treatments have also been applied to the VR of NMAD in solution.[7,15,32,79,80] While the most popular of these methods based on Fermi's golden rule plus use of classical force−force correlation functions gives decay times of about ≈2 orders of magnitude larger than the experiment,[58] recent theoretical improvements have been shown to give more accurate results.[67,81] VR lifetimes calculated by Straub et al.,[81] in particular, are found to be in good agreement with those provided experimentally by Hochstrasser et al.[4] Straub et al.[81] model the VR process as a multistep reaction and use non-Markovian time-dependent perturbation theory[31] with the Neumann−Liouville equation and the third-order Fermi resonance parameters to determine the mode-to-mode energy flow rate constants. Perturbation treatments clearly indicate that the correct simulation of the vibrational energy relaxation of the NMAD in solution requires the consideration of quantum effects such as the existence of discrete levels in the solute, a feature which become especially important for the amide I mode relaxation for which the spacing between vibrational levels is significantly larger than k_BT. These methods are, however, limited to the short time regime dynamics and are not able to provide therefore a complete description of the whole relaxation process.

In mode-specific vibrational energy relaxation processes of solute molecules in condensed phase, the degrees of freedom requiring a quantum description are usually localized in the solute molecule, which facilitates the realization of a well-defined initial partition of the whole system in quantum and classical subsystems. Hybrid quantum-classical methods[22,82−85] are then a highly intuitive tool for the study of these processes since they proceed through simultaneous propagation of the solute quantum state and the classical degrees of freedom. Classical coordinates that couple to the vibrational quantum states can then be identified and thereafter connected with different intramolecular and intermolecular energy transfer pathways, thus giving us a deep understanding of the molecular mechanism of the relaxation. Surface-hopping[86−89] and mean field[90−94] methods are the two most widely used hybrid quantum/classical methods approaches able to treat interactions between quantum and classical subsystems in a self-consistent way, and both have been applied to the study of VR and IVR in van der Waals clusters and condensed phases.[85] Also recently, the so-called mixed quantum-classical Liouville method has been used to describe vibrational energy redistribution[95−98] (VER). Within this approach, VER is described as a nonequilibrium process involving solvation on different vibrational adiabatic potential energy surfaces and nonadiabatic transitions between them. Since this method does not rely on a perturbative treatment of the interaction between the relaxing mode and the bath modes, it allows for a direct analysis of the VER mechanism.

Among the surface-hopping approaches, vibrational molecular dynamics with quantum transitions (MDQT) has been implemented and successfully used to deal with vibrational predissociation, IVR, and fragmentation dynamics of van der Waals clusters consisting of a dihalogen molecule surrounded by a number of rare gas atoms.[99−104] This method relies on the MDQT treatment of electronic transitions developed by Tully[87,105] as adapted to vibrational transitions, in which the vibration of the diatomic molecule treated quantum-mechanically and the remaining degrees of freedom are treated classically, and it provides lifetimes and final state distributions which can be properly used to develop kinetic schemes to interpret the VR process. The vibrational MDQT method has also been applied to VR in the condensed phase, mostly with diatomic molecules in solution.[106−109]

The aim of this work is to investigate the vibrational energy relaxation of the amide I mode of the NMAD molecule in aqueous solution (D_2O) using vibrational hybrid quantum/classical MD. For this purpose, we develop the implementation of the vibrational MDQT method to deal in general with one normal mode of the solute polyatomic molecule being treated quantum mechanically and the remaining intra- and intermolecular degrees of freedom being treated classically. The paper is organized as follows. In Section 2 we describe the specific issues concerning the novel implementation of the vibrational MDQT method, the way in which the transient energy content of the vibrational modes of the solute is evaluated using INMs, and the computational details employed in this work. In Section 3 we present and discuss the results obtained for the VR of the NMAD amide I mode in deuterated water solution, comparing them with previous classical MD calculations of the system. Conclusions are given in Section 4.

2. METHODOLOGY

2.1. Vibrational MDQT. Nonequilibrium hybrid quantum/classical surface-hopping approaches have been extensively used to describe VR processes.[99,101−104,106,107,110] The general description of the method can be found elsewhere,[85,99] so we concentrate here on the specific features when it is applied to the VR of a quantal normal mode, Q_k, of a polyatomic solute molecule like NMAD, dissolved in a liquid like D_2O. The Hamiltonian of the system can then be written as follows

$$H(Q_k, \mathbf{R}) = H_q(Q_k) + H_{cl}(\mathbf{R}_{cl}) + V_{int}(Q_k, \mathbf{R}_{cl}) \quad (1)$$

where $H_q(Q_k)$ is the one-dimensional (1D) quantum harmonic oscillator Hamiltonian of the vibrational normal mode Q_k, given by

$$\hat{H}_q(Q_k) = -\frac{\hbar^2}{2}\frac{\partial^2}{\partial Q_k^2} + \frac{1}{2}\lambda_k \hat{Q}_k^2 \quad (2)$$

$H_{cl}(\mathbf{R}_{cl})$ is the Hamiltonian of the remaining classical coordinates, $\mathbf{R}_{cl}$, and $V_{int}(Q_k,\mathbf{R}_{cl})$ is the interaction potential that couples the quantum and classical degrees of freedom. The classical degrees of freedom, $\mathbf{R}_{cl}$, include all of the solvent coordinates, the translational and rotational coordinates of the solute molecule, given specifically by the center of mass vector $\mathbf{R}_{CM}$ and the quaternions $\mathbf{q} = (q_1,q_2,q_3,q_4)$, and all of the vibrational coordinates of the solute, excluding the quantal normal mode Q_k. Details concerning the classical equations of motions can be found in refs 68 and 69, including the use of the

dx.doi.org/10.1021/jp210727u | J. Phys. Chem. B 2012, 116, 2969−2980

rigid rotor model for the NMAD molecule which has been validated in previous classical MD simulations.[68]

In our earlier nonequilibrium MD simulations[68,69,78] we also used the equilibrium normal modes (ENMs), $\mathbf{Q}^{e} = (Q_1^{e},...,Q_N^{e})$ of NMAD as propagation coordinates. These coordinates do not provide, however, a fully separable description of the molecule in solution at room temperature due to the strong couplings among the ENMs that emerge when the molecule explores configurations which are far away from the equilibrium geometry. In this work we use as propagation coordinates instead the INMs of NMAD calculated at the initial time, $t = 0$, of the simulations, just when the quantal normal mode of the solute Q_k is excited. These initial INMs $\mathbf{Q}^{INM_0} = (Q_1^{INM_0},...,Q_N^{INM_0})$ provide a proper description of the quantal vibrational normal mode $(Q_k^{INM_0})$ excited with one vibrational quantum, decoupled up to second order from the remaining classical normal modes of the solute. The initial vibrational energy located in the quantum subsystem is therefore $3\hbar\omega_k^{INM_0}/2$, where $\omega_k^{INM_0}$ is the vibrational frequency of the quantal $Q_k^{INM_0}$ mode of NMAD, with $k = 23$ corresponding to the amide I mode. The value of the 23th INM_0 frequency varies depending on the specific instantaneous initial configurations used to start the individual trajectories, and the average of this frequency provides therefore the mean quantum vibrational energy initially deposited in the system.

The initial INM_0's are obtained by diagonalizing the $N \times N$ ENM Hessian $\mathbf{K}^{ENM}$ matrix at $t = 0$.[68,78] Both sets of modes are therefore related by the eigenvector matrix $\mathbf{L}^{INM_0}$ as follows

$$\mathbf{K}^{ENM}(0)\mathbf{L}^{INM_0} = \mathbf{L}^{INM_0}\mathbf{\Lambda}^{INM_0} \tag{3}$$

where $\mathbf{\Lambda}^{INM_0}$ is the diagonal eigenvalue matrix whose elements, $\lambda_i^{INM_0}$, are related to the INM_0 vibrational frequencies by $\nu_i^{INM_0} = (\lambda_i^{INM_0})^{1/2}/2\pi$. The assignment of the INM_0's in terms of the ENMs is performed using the so-called Min-Cost algorithm,[69,78] which maximizes the trace of the overlap matrix with elements $(l_{ij}^{INM_0})^2$ as described in refs 69 and 78.

The time evolution of the wave function $|\psi(t)\rangle$ accounting for the vibrational motion of the quantal coordinate $Q_k^{INM_0}$ is governed by the time-dependent Schrödinger equation

$$i\hbar\frac{\partial|\psi(t)\rangle}{\partial t} = (\hat{H}_q(Q_k^{INM_0}) + \hat{V}_{int}(Q_k^{INM_0}, \mathbf{R}_{cl}))|\psi(t)\rangle \tag{4}$$

which is solved by expanding the time-dependent wave function $|\psi(t)\rangle$ in terms of the diabatic eigenstates $|v\rangle$ of the $\hat{H}_q$ harmonic oscillator Hamiltonian with energy E_v as follows

$$|\psi(t)\rangle = \sum_v c_v(t)|v\rangle \tag{5}$$

The usefulness of the diabatic states in hybrid quantum/classical surface-hopping calculations of VR processes has been demonstrated in a number of studies.[99,102,111−113] In this case, previous classical MD simulations of the VR of the NMAD amide I mode in D_2O solution have shown that this mode widely preserves its identity along the simulation,[78] as stated by the standard deviation of its frequency, which remains below 0.5%.[68] The couplings of the amide I mode with the rest of NMAD modes are therefore expected to be relatively small, thus validating the use of the corresponding diabatic states as a natural representation of the quantum degree of freedom.

The substitution of eq 5 into eq 4 gives

$$i\hbar\dot{c}_{v'}(t) = \sum_v c_v(t)H_{v'v} \tag{6}$$

where

$$H_{v'v} = \langle v'|\hat{H}_q(Q_k^{INM_0}) + \hat{V}_{int}(Q_k^{INM_0}, \mathbf{R}_{cl})|v\rangle = E_v\delta_{v'v} + \langle v'|\hat{V}_{int}(Q_k^{INM_0}, \mathbf{R}_{cl})|v\rangle \tag{7}$$

The diabatic couplings in this expression can be efficiently calculated all along the hybrid simulations by expanding them in a Taylor series of the quantum coordinate $Q_k^{INM_0}$ about its equilibrium, $Q_k^{INM_0} = 0$, value as follows[112,113]

$$\langle v'|\hat{V}_{int}(Q_k^{INM_0}, \mathbf{R}_{cl})|v\rangle = V_{int}(0, \mathbf{R}_{cl})\delta_{v,v'} + K_{Q_k^{INM_0}}\langle v'|\hat{Q}_k^{INM_0}|v\rangle + K_{(Q_k^{INM_0})^2}\langle v'|(\hat{Q}_k^{INM_0})^2|v\rangle + ... \tag{8}$$

where K are the expansion coefficients which are evaluated at the current values of the classical coordinates using a finite difference method. In practice it suffices to include up to the quadratic terms in these expansions to reach convergence.[112,113]

In the present implementation of the vibrational MDQT method, the classical degrees of freedom evolve on the vibrational energy surface created by a single vibrational state $|v\rangle$ of the quantal $Q_k^{INM_0}$ harmonic mode. The Hamilton equations for the classical variables are then

$$\dot{\mathbf{R}}_{cl} = \mathbf{P}_{\mathbf{R}_{cl}}/m_{\mathbf{R}_{cl}} \tag{9}$$

$$\dot{\mathbf{P}}_{\mathbf{R}_{cl}} = -\nabla_{\mathbf{R}_{cl}}H_{cl}(\mathbf{R}_{cl}) - \langle v|\nabla_{\mathbf{R}_{cl}}\hat{V}_{int}(Q_k^{INM_0}, \mathbf{R}_{cl})|v\rangle \tag{10}$$

where the first and second terms on the right-hand side of eq 10 corresponds, respectively, to the classical forces, $\mathbf{F}_{\mathbf{R}_{cl}}$, and to the averaged classical/quantum interactions, with the latter being computed using a Taylor expansion similar to that used to evaluate the diabatic couplings in eq 8. In this case it suffices to include up to linear terms in the expansion to reach convergence.

In the vibrational MDQT method[87] classical trajectories can hop from one vibrational state to another at each propagation time with the hop probabilities governed by the relative change over time of the coefficients of the vibrational wave function $|\psi(t)\rangle$. A preliminary analysis of the time evolution of the quantum populations of the NMAD amide I mode in D_2O solution reveals the occurrence of short-time oscillations unrelated to the global relaxation process. These oscillations give large short-time values for the $|1\rangle \rightarrow |0\rangle$ hopping probabilities. The significantly larger value of the amide I vibrational quantum with respect to the thermal energy hinders then the possibility of any subsequent $|0\rangle \rightarrow |1\rangle$ hop back. As a consequence, these classical forbidden transitions leads to unsuitable ultrafast divergences between the averaged quantum and classical populations. An example of these divergences is shown in Figure 1, where the quantum, $|c_v(t)|^2$, and classical populations of the NMAD amide I mode calculated using the hopping probabilities during the first 80 fs of a typical simulation are plotted. While different strategies have been proposed to overcome this drawback,[114,115] as far as the

dx.doi.org/10.1021/jp210727u | J. Phys. Chem. B 2012, 116, 2969−2980

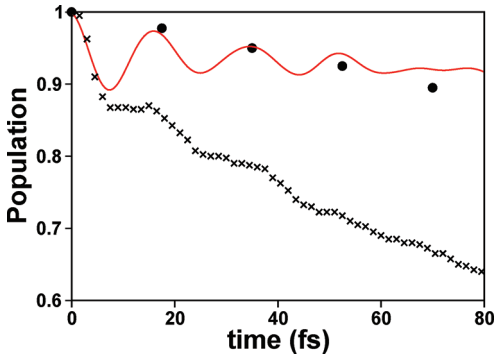

Figure 1. Average quantum (red line) and classical populations for the $v = 1$ VR of the amide I mode obtained by evaluating the hopping probabilities at every classical time step Δt (crosses) and using eq 11 (circles).

vibrational MDQT method is concerned we found that this problem can be properly solved by evaluating the probability of the quantum transition from the current vibrational state $|v\rangle$ to any other state $|v'\rangle$ at every period of short-time oscillation using the expression[105]

$$g_{v\to v'} = \frac{\int_t^{t+\delta} 2\mathrm{Im}(c_v(t')c_{v'}^*(t'))H_{v'v}\mathrm{d}t'}{|c_v(t)|^2} \tag{11}$$

where the integral is evaluated numerically using a δ values equal to $35\Delta t$ which is found to match well with the average short-time oscillation period of 17.5 fs obtained using a classical time step $\Delta t = 0.5$ fs. As observed in Figure 1 the calculation of the hopping probabilities using eq 11 (black dots) ensures a better short-time agreement between classical and quantum populations.

2.2. Hybrid INM Analysis. The definition of the ENMs based on the second-order expansion of the potential energy function of the isolated solute molecule about its equilibrium configuration makes them unsuitable to express the vibrational energy of the solvated molecule as the sum of individual harmonic contributions at room temperature.[78] As for the INM_0's, they provide a decoupled description of the vibrational motions of the molecule at the initial configurations of the VR which validates them to achieve a proper initial definition of the quantum and classical subsystems as required in the hybrid quantum/classical approach. Structural perturbations emerging throughout the dynamics of the system introduce, however, strong couplings among the INM_0's, making it quite difficult to quantify the energy stored in each individual normal mode. To address this problem we use the INMs, INM_t's, evaluated at each propagation time, as was done successfully in our previous studies on this system.[68,69,78] The INM_t's are assigned using the Min-Cost algorithm with the ENMs as templates, to track their identities as the whole system evolves with time.

As previously reported,[69] there are INM_0's (or INM_t's) which cannot be unambiguously assigned to a single ENM and are therefore gathered in groups according to their nearly degenerated time-averaged vibrational frequencies. In order of ascending frequency, we have then first the group a_1 of modes, composed of the 11th to 15th INMs, which are mainly formed by combinations of the rocking methyl ENMs and a backbone ENM mode. Then we have group a_2, composed of the 16th to 20th INMs with the bending methyl ENMs contributing the most. Next comes group b_1, formed by the 25th and 26th INMs which are composed essentially of the C−H stretches ($\nu_s(CH_3)$) excited during in the simulations, and finally we have group b_2, formed by the 27th to 30th INMs, made up basically of the more energetic stretching methyl ENMs. A complete list of the INMs and their assignments in terms of the ENMs can be found in ref 69.

Since the $Q_k^{INM_0}$ mode is treated quantum-mechanically and the rest of modes $Q_j^{INM_0}$, $j \neq k$, are treated classically, it is important to stress that the INM_t's are really hybrid quantum/classical modes whose position $\hat{Q}_i^{INM_t}$ and momentum $\hat{P}_i^{INM_t}$ operators are obtained by projecting them onto the $\boldsymbol{Q}^{INM_0}$ basis set as follows

$$\hat{Q}_i^{INM_t}(t) = \sum_{\substack{j=1 \\ j\neq k}}^{N} g_{ji} Q_j^{INM_0}(t) + g_{ki}\hat{Q}_k^{INM_0} \tag{12}$$

$$\hat{P}_i^{INM_t}(t) = \sum_{\substack{j=1 \\ j\neq k}}^{N} g_{ji} P_j^{INM_0}(t) + g_{ki}\hat{P}_k^{INM_0} \tag{13}$$

where $\hat{Q}_k^{INM_0}$ and $\hat{P}_k^{INM_0}$ are the position and momentum operators corresponding to the $Q_k^{INM_0}$ quantum mode, and g_{ij} is the dot product of $Q_j^{INM_t}$ and $Q_j^{INM_0}$. Accordingly, the vibrational energies of the individual INM_t's can be written in the form

$$E_i^{INM_t} = \frac{1}{2}\langle v|(\hat{P}_i^{INM_t})^2|v\rangle + \frac{1}{2}\lambda_i^{INM_t}\langle v|(\hat{Q}_i^{INM_t} + a_i^{INM_t})^2|v\rangle \tag{14}$$

where $a_i^{INM_t}$ are the coordinate shifts.[68] The substitution of eqs 12 and 13 into eq 14 leads to

$$E_i^{INM_t} = \frac{1}{2}\lambda_i^{INM_t}(a_i^{INM_t})^2(1 - g_{ki}^2) + \frac{1}{2}g_{ki}^2\langle v|(\hat{Q}_k^{INM_0})^2|v\rangle + \frac{1}{2}g_{ki}^2\langle v|(\hat{P}_k^{INM_0})^2|v\rangle + T_i^{INM_t,cl}(t) \tag{15}$$

where

$$T_i^{INM_t,cl}(t) = \frac{1}{2}\sum_{\substack{j=1 \\ j\neq k}}^{N} g_{ji}^2(\dot{Q}_j^{INM_0}(t))^2 + \frac{1}{2}\sum_{\substack{j=1 \\ j\neq k}}^{N}\sum_{\substack{m=1 \\ m\neq j,k}}^{N} g_{ji}g_{mi}\dot{Q}_j^{INM_0}(t)\dot{Q}_m^{INM_0}(t) \tag{16}$$

Note that a factor $(1 - g_{ki}^2)$ is included in the first term on the right side of eq 15 for the values of the potential energies of the individual INM_t's to asymptotically reach their correct equilibrium values, obtained as a weighted average of the classical and quantum INM_0's.

After discussing the hybrid INM_t's, it remains to specify how the energy is conserved at the quantum hops. In diabatic vibrational MDQT calculations this is achieved by matching the

components of the classical momenta in the direction of the diabatic coupling vector as follows[99]

$$\mathbf{P'}_{\mathbf{R}_{cl}} = \mathbf{P}_{\mathbf{R}_{cl}} + \gamma \mathbf{F}^{\nu\nu'}_{\mathbf{R}_{cl}} \quad (17)$$

where

$$\mathbf{F}^{\nu\nu'}_{\mathbf{R}_{cl}} = \langle \nu | \nabla_{\mathbf{R}_{cl}} V_{int}(Q_k^{INM_0}, \mathbf{R}_{cl}) | \nu' \rangle \quad (18)$$

Here $\mathbf{P}_{\mathbf{R}_{cl}}$ and $\mathbf{P'}_{\mathbf{R}_{cl}}$ are the classical momenta before and after the hop, and the value of γ is obtained by imposing energy conservation. Previous nonequilibrium classical MD calculations[68] of the VR of the NMAD amide I mode in D_2O solution have shown unrealistic excitations of normal modes with vibrational frequencies higher than that of the parent mode occur during the relaxation process. It is possible to minimize this unphysical flow of energy by restricting the energy transfer during hops to those INM_t whose frequencies lie below the amide I mode frequency. To achieve this, we calculate first the forces exerted on the hybrid INM_t's from the forces exerted on the classical INM_0's using the expression

$$F^{\nu\nu'}_{Q_i^{INM_t}} = \sum_{\substack{j=1 \\ j\neq k}}^{N} g_{ji} F^{\nu\nu'}_{Q_j^{INM_0}}$$

$$i = 1, ..., k-1, k+1, ...N \quad (19)$$

Next we remove the INM_t forces acting on the hybrid modes with frequencies higher than the amide I mode frequency, and finally we calculate back the forces on the INM_0's using the inverse relation to eq 19. In other words, we recalculate the forces acting on the classical modes in such a way that the contributions to the change of the momenta of the hybrid modes above the frequency threshold are set to zero.

2.3. Computational Details. We have carried out MD simulations of one NMAD molecule surrounded by 251 D_2O molecules, all of them placed in a cubic box with a length of 1.975 nm, chosen to reproduce the experimental density of the system[116] (ρ = 1.10436 g/cm^3). The AMBER force field[117] is employed to model the solute NMAD ($H_3C-COND-CH_3$) and the flexible TIP3P water model with doubled hydrogen masses included in the CHARMM[118] force field to represent the D_2O molecules. Subroutines of the TINKER modeling package[119] are also used in our code to evaluate the forces and the potential energy function. Periodic boundary conditions are imposed to simulate the bulk system, and a cutoff of 10 Å is applied to nonbonded interactions.

The classical equations of motion are integrated using the leapfrog algorithm,[120,121] with a time step of 0.5 fs. Quantum-mechanical equations are solved using an Adams-Moulton propagator with 4.0×10^{-7} tolerance to ensure norm conservation. To evaluate the diabatic coupling terms $\langle \nu' | \hat{V}(Q_k^{INM_0}, \mathbf{R}_{cl}) | \nu \rangle$ appearing in eq 8 as many times as required in the interpolations performed by the multistep quantum propagator, we use a recently proposed algorithm based on the use of a parabolic interpolation function.[122]

We have performed 24 NVT equilibrium MD simulations of 1250 ps initialized using random velocities. The temperature was maintained at a mean value of 300 K by coupling to a thermal bath[123] with a time constant of 0.1 ps. During these trajectories, the amide I mode (23rd ENM) was held frozen at its equilibrium value, and the last 500 ps were used to collect equilibrated configurations at 20 ps intervals. Thus, 600 sets of positions and momenta were stored for use as initial conditions for the subsequent nonequilibrium MD simulations, which were performed in turn in the NVE ensemble to avoid any influence of velocity scaling on the results. The ENMs were used to propagate the NMAD vibrations during the equilibration period and the INM_0's to propagate the NMAD vibrations during the simulations of the relaxation process. The nonequilibrium MD simulations were started from these initial configurations by setting the wave function $|\psi(t)\rangle$ that characterizes the vibrational motion in the quantum coordinate $Q_{23}^{INM_0}$ equal to the first excited vibrational state $|1\rangle$. A number of 600 hybrid quantum/classical trajectories of 40 ps were propagated to attain reasonable statistics in all of the quantities reported.

3. RESULTS AND DISCUSSION

Previous studies have shown that the hybrid quantum/classical methods may not provide the equilibrium Boltzmann quantum state populations in the long time limit,[23,24,88,111,112,124−132] which supposes a serious limitation to their applicability in simulations of VR of solute molecules in solution. It is therefore important to consider first the behavior of the populations of the vibrational states of the amide I mode ($Q_{23}^{INM_0}$) of the NMAD molecule during the VR of it in liquid D_2O. We note then that the vibrational quantum of this mode is much higher than the thermal energy ($\hbar\omega_{23}^{INM_0} \gg k_B T$), so only the ground state is expected to be significantly populated at equilibrium. The high energy gap between the ground state and the first excited state means, in addition, that the $|0\rangle \rightarrow |1\rangle$ MDQT hops are, in practice, energetically forbidden, so once a trajectory relaxes to the ground $\nu = 0$ amide I vibrational state it remains trapped there. As a consequence, the classical populations tend asymptotically toward their right equilibrium Boltzmann distributions, as observed in Figure 2.

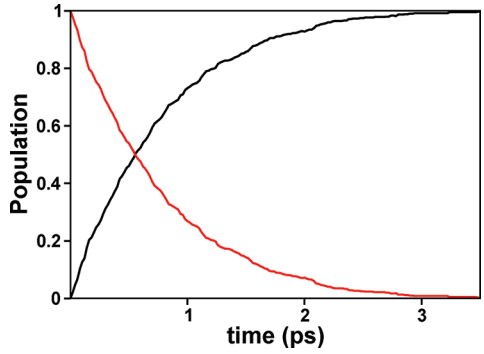

Figure 2. Time evolution of the classical populations of the ground state (black line) and the first excited state (red line) of the NMAD amide I mode in liquid D_2O.

Let us focus now on the VR of the NMAD amide I mode in D_2O solution. In Figure 3 we show the evolution in time of the normalized vibrational energy of this mode, relative to its equilibrium value, along with the evolution of the energy extracted from our previous nonequilibrium classical MD simulations[68] and the experimental one.[4,54] The average initial excitation energy of the amide I mode is 1692.7 cm^{-1}, and as observed in Figure 3, it decays in the hybrid simulations until reaching its equilibrium value in a period of time similar to that for populations (see Figure 2). The hybrid MDQT decay is also significantly faster than that obtained from the classical MD

dx.doi.org/10.1021/jp210727u | J. Phys. Chem. B 2012, 116, 2969−2980

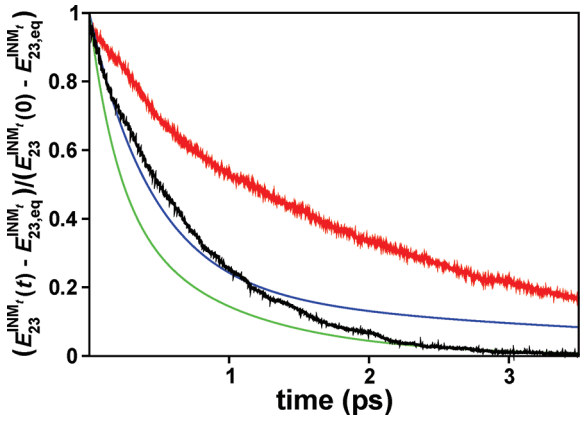

Figure 3. Normalized time evolution of the vibrational energy of the NMAD amide I mode in D_2O solution with respect to its equilibrium value, obtained from hybrid simulations (black line) and classical[68] (red line) simulations, and from experiments conducted by Hochstrasser et al.[4] (blue line) and by Tokmakoff et al.[54] (green line).

simulations and closer to those reported experimentally by Hochstrasser et al.[4] and Tokmakoff et al.,[54] showing a better agreement with the Hochstrasser data. Our hybrid results thus confirm that the inclusion of quantum effects in nonequilibrium MD do have an accused effect on the VR of the NMAD amide I mode in D_2O solution. This is consistent with previous findings reported by Stock from the comparison of classical and quantum-mechanical perturbation theory[133] based on a system-bath model with cubic couplings. Stock thus shows that the inclusion of an adequate quantum correction factor enhances the amide I relaxation rate obtained by classical nonequilibrium MD simulations. Since previous studies have demonstrated that the initial fast IVR relaxation of the amide I mode proceeds mainly through third-order couplings,[65,68] the improvement achieved by the present quantum description of this mode can be mainly attributed to the different way in which these anharmonic couplings are considered in the classical and the quantum treatments.

The hybrid decay curve is found to be well-reproduced by the single-exponential function

$$\frac{E_{23}^{\mathrm{INM}_t}(t) - E_{23,\mathrm{eq}}^{\mathrm{INM}_t}}{E_{23}^{\mathrm{INM}_t}(0) - E_{23,\mathrm{eq}}^{\mathrm{INM}_t}} = e^{-t/\tau_{\mathrm{rel}}} \tag{20}$$

where τ_{rel} is the relaxation time and where the subscript eq stands for the energy of the INM_t at equilibrium. This is in contrast with the biexponential function which was used to fit the results from the MD simulations[58,68] and also to fit the experimental data.[4,54] The values of the parameters obtained in all these fits show, however, large uncertainties, evidencing the difficulties arising in obtaining a unique set of adjustable parameters that uniquely reproduce the amide I mode decay curve. While the results from the hybrid simulations can also be fitted reasonably well to a biexponential function, with otherwise larger uncertainties, we prefer to keep the single-exponential fit for simplicity. In Table 1 we give the hybrid relaxation time of the amide I mode thus obtained, together with the relaxation times extracted from the previous theoretical and experimental studies. To make a proper comparison of the hybrid single-exponential decay time (τ_{rel} = 0.73 ps) with the biexponential decay times, we calculate the relaxation time, T_1, for the latter at which the initial vibrational energy decreases in a factor of $1/e$.

Table 1. VR Times (in picoseconds) of the Amide I Mode Obtained by Fitting to Mono- And Biexponential Decay Functions[a]

		τ_1 (c_1)	τ_2 (c_2)	T_1
experimental	Hochstrasseret al.[b]	0.45 (0.80)	4.00 (0.20)	0.63
	Tokmakoff et al.[c]	0.20 (0.55)	0.86 (0.45)	0.39
MDQT		0.73 (1.00)		0.73
MD	Bastida et al.[d]	1.55 (0.80)	4.01 (0.20)	1.76
	Nguyen and Stock[e]	1.90 (0.80)	13.3 (0.20)	2.60
second-order perturbation theory[f]		0.43 (1.00)		0.43
		0.60 (1.00)		0.60
		0.54 (1.00)		0.54
		0.93 (1.00)		0.93

[a]The c_i parameters are the normalized weights (see eq 23). [b]Reference 4. [c]Reference 54. [d]Reference 68. [e]Reference 58. [f]Reference 65.

We observe then in Table 1 that the hybrid quantum/classical simulations provide substantially shorter relaxation times than those from the classical MD simulations, and in closer agreement with experiments. Table 1 also shows that similar improvements in the relaxation times have been previously reported by Fujisaki et al.[62] taking into account the quantum effects through second-order perturbation theory.

Let us analyze next the amide I mode relaxation pathways. The vibrational MDQT method allows us to calculate accurately the amount of energy transferred at the quantum hops from the initially excited quantum amide I mode to any other classical degree of freedom using the classical momenta values calculated before and after the hops (see eq 17). Interestingly, we find that the translational and rotational degrees of freedom of NMAD, as a whole, do not receive significant amounts of energy and that only 3% ($\approx$ 60 cm^{-1}) of the vibrational energy initially deposited in the quantal amide I mode is transferred to the solvent, with the rest of it therefore being distributed among the other vibrational NMAD modes, in agreement with previous theoretical and experimental investigations.[55,68,69] Accordingly, the relaxation of the NMAD amide I mode is essentially an IVR process with a residual contribution of intermolecular transfer of energy to the solvent molecules. In Table 2 we give the average energy transferred from the amide I mode to the different INM_t's in the hops. It is interesting to note that the average energy lost by the parent amide I mode, of 1465 cm^{-1}, is about 230 cm^{-1} lower than the initial average energy deposited in this mode of 1692 cm^{-1}. This energy mismatch arises from the mixed quantum/classical nature of the hybrid amide I (23rd INM_t) mode, whose dominant contribution over the initial INMs ($\approx$ 90%) is that from the initial quantum 23rd INM_0, with the rest of the contributions coming from the classical INM_0's. Accordingly, the hops from the 23rd INM_0 quantum state do not necessarily involve the transfer of the same amount of energy as the hops from the hybrid 23rd INM_t. Among the INM_t's that receive the largest amounts of energy directly from the amide I mode are the first ($\tau(CH_3)$), the second ($\tau(CH_3)$), and the third (τ(CN)) low-frequencies modes, the sixth (amide V) and eighth (amide VI) modes, and the group a_1 ($r(CH_3)$ + ν(CN)) of modes.[69] The energy received by the group a_2 (mostly bending methyl ENMs) is distributed into 30 cm^{-1} per mode on average, a significantly smaller energy quantity than that received by the aforementioned modes. Finally, we should

dx.doi.org/10.1021/jp210727u | J. Phys. Chem. B 2012, 116, 2969–2980

Table 2. Vibrational Energy (in cm^{-1}) Transferred from the Amide I Mode to the INM_t's of the NMAD Molecule at the Hops

*i*th INM	$\langle \Delta E_i^{INM_t} \rangle_{hop}$	label[a]
1	114.1 ± 247.2	$\tau(CH_3)$
2	104.3 ± 223.8	$\tau(CH_3)$
3	83.4 ± 178.9	τ(CN)
4	36.9 ± 125.8	δ(CNC)
5	45.6 ± 112.8	δ(CCN)
6	93.8 ± 201.4	amide V
7	41.3 ± 116.3	amide IV
8	186.1 ± 294.8	amide VI
9	23.4 ± 84.4	ν(CC)
10	16.8 ± 80.6	amide III
group a_1[b]	541.6 ± 427.1	$r(CH_3) + \nu$(CN)
group a_2[b]	151.0 ± 249.2	$\delta(CH_3)$
21	8.8 ± 95.3	$\delta_s(CH_3)$N
22	−17.1 ± 71.2	amide II
23	−1464.7 ± 163.6	amide I
24	−1.4 ± 3.0	amide A
group b_1[b]	−4.8 ± 8.6	$\nu_s(CH_3)$
group b_2[b]	−15.1 ± 15.5	$\nu(CH_3)$

[a] τ = torsion, δ = bending, ν = stretching, r = rocking, a = asymmetric, and s = symmetric. [b] Groups a_1, a_2, b_1 and b_2 are formed by 5, 5, 2, and 4 modes, respectively.

note that no significant amount of energy is transferred in the hybrid simulations to the amide II mode (22th INM_t), in agreement with recent experimental data obtained using two-color femtosecond vibrational spectroscopy.[56]

Analysis of the evolution of the vibrational energy of each individual INM_t allows us to identify the roles that they play as intermediate modes during the VR process, after excitation of the NMAD amide I mode. It is important to stress here that since the amount of energy stored in each INM_t depends on both their relative excitation and relaxation times, the maximum energy stored in them will not necessarily coincide with the amount of energy transferred at the hops (see Table 2). In Figures 4 and 5 we show the time evolution of the average vibrational energies relative to their equilibrium values for all the INM_t's which accumulate a significant amount of energy during the relaxation process. The vertical dashed line delimits the first relaxation stage, in which the largest part of the excess of vibrational energy deposited in the amide I is released, in a time of roughly $2\tau_{rel}$ = 1.46 ps. As observed, all of the modes shown in Figure 4 undergo similarly fast excitations within the time interval in which the amide I mode relaxes, whereas subsequent relaxation of these modes becomes faster for the first, second, and third low frequency modes. Similar fast excitations are observed in Figure 5 (note the different time scale) for the higher frequency groups of modes a_1, a_2, and b_1. In contrast, excitation of the ninth, tenth, and the group b_2 of modes is slower, so their vibrational energy curves reach the maxima at substantially longer times. This is in agreement with the small direct energy transfer from the amide I mode into these modes (see Table 2), indicating that they are being excited from some intermediate modes. All of the mid- and high-frequency modes shown in Figure 5 relax more slowly than the low-frequency modes included in Figure 4. We also note that a comparative smaller amount of energy is stored in the seventh and the group a_2 of modes as a consequence of the little energy received by these modes from the amide I mode.

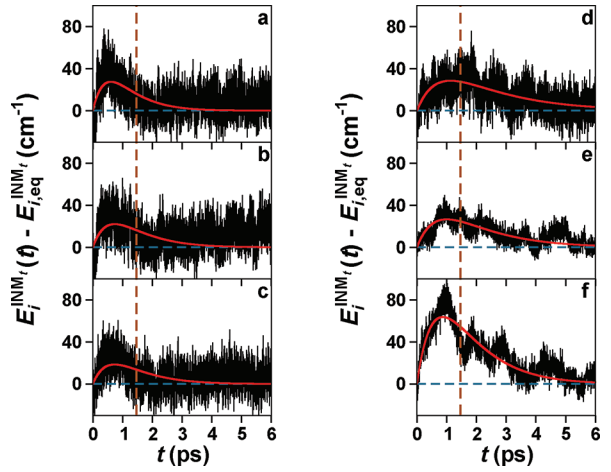

Figure 4. Time evolution of the vibrational energy of the (a) first, (b) second, (c) third, (d) sixth, (e) seventh, and (f) eighth INM_ts (black lines) extracted from the hybrid MDQT simulations, with the adjustment curves to eq 21 superimposed. The limit of the first stage at 1.46 ps is indicated by the brown vertical dashed line.

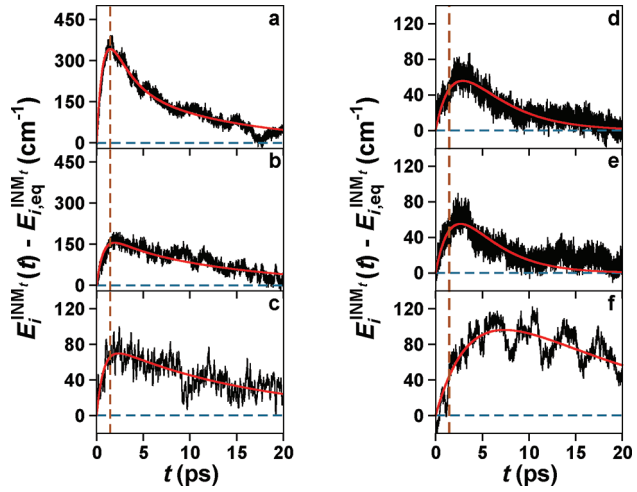

Figure 5. Time evolution of the vibrational energy of the (a) a_1, (b) a_2, and (c) b_1 INM_t groups, (d) ninth and (e) tenth INM_t, and the (f) group b_2 (black lines), with the adjustment curves to eq 21 superimposed. The limit of the first stage at 1.46 ps is indicated by a brown vertical dashed line.

The fast excitation of the group b_1 ($\nu_s(CH_3)$) of modes during the first relaxation stage (see Figure 5c) could be due, in principle, to a fast direct transfer of energy from the amide I mode. The results reported in Table 2 show, however, that this is not the case. Previous experimental and theoretical studies have demonstrated that the stretching $\nu_s(CH_3)$ modes (group b_1) and the bending $\delta(CH_3)$ modes of the methyl groups (group a_2) are strongly coupled to each other and that these couplings promote a fast interchange of energy between them.[15,55,69,134−138] Group b_1 of modes therefore receives energy because of its strong mixing with group a_2, rather than by direct transfer from the amide I mode. We should note that these two mechanisms cannot be distinguished by classical MD simulations, since these simulations do not provide the information needed to discern between the pathways that the energy directly released by the parent mode follows (see Table 2).

dx.doi.org/10.1021/jp210727u | J. Phys. Chem. B 2012, 116, 2969−2980

Table 3. Fitted Parameters for the VR of Different INM$_t$'s of NMAD, Including Relaxation and Excitation Times (in picoseconds), Amplitudes (in %), and Parameter A (in cm^{-1})

$E_i^{\mathrm{INM}_t} = A(a_{\mathrm{rel}}e^{-t/\tau_{\mathrm{rel}}} + a_{\mathrm{rel}}{}'e^{-t/\tau'_{\mathrm{rel}}} - e^{-t/\tau_{\mathrm{exc}}})$	τ_{exc}	τ_{rel}	a_{rel}	$\tau_{\mathrm{rel}}{}'$	$a_{\mathrm{rel}}{}'$	A	time interval	constraints
group a_1 ($r(CH_3)$ + ν_s(NC))	0.73	2.00	66	12.31	34	707	t < 40 ps	τ_{exc}, τ_{rel}
group a_2 ($\delta(CH_3)$)	0.73	2.00	28	14.00	72	233	t < 40 ps	τ_{exc}, τ_{rel}, $\tau_{\mathrm{rel}}{}'$
$E_i^{\mathrm{INM}_t} = A(e^{-t/\tau_{\mathrm{rel}}} - e^{-t/\tau_{\mathrm{exc}}})$	τ_{exc}	τ_{rel}	A	time interval	constraints			
first INM ($\tau(CH_3)$)	0.73	0.74	6776	t < 3 ps	τ_{exc}			
second INM ($\tau(CH_3)$)	0.73	0.75	4400	t < 3 ps	τ_{exc}			
third INM (τ(CN))	0.73	0.74	7845	t < 3 ps	τ_{exc}			
sixth INM (amide V)	0.73	1.87	85	t < 5 ps	τ_{exc}			
seventh INM (amide IV)	0.73	1.43	109	t < 5 ps	τ_{exc}			
eighth INM (amide VI)	0.73	1.05	480	t < 5 ps	τ_{exc}			
ninth INM (ν(CC))	2.00	3.27	332	t < 10 ps	τ_{exc}			
tenth INM (amide III)	2.00	3.62	256	t < 10 ps	τ_{exc}			
group b_1 ($\nu_s(CH_3)$)	0.73	16.0	85	t < 40 ps	τ_{exc}			
group b_2 ($\nu(CH_3)$)	4.06	15.6	208	t < 40 ps				

The time evolution of most of the intermediate modes shown in Figures 4 and 5 can be rationalized by considering these modes modes as midrange M modes in the sequential kinetic mechanism $P \rightarrow M \rightarrow L$ in which P is the parent amide I mode and L are the lower-frequency modes. According to this mechanism, the evolution over time of the energy is given by

$$E_i^{\mathrm{INM}_t}(t) - E_{i,\mathrm{eq}}^{\mathrm{INM}_t} = A(e^{-t/\tau_{\mathrm{rel}}} - e^{-t/\tau_{\mathrm{exc}}}) \quad (21)$$

where τ_{exc} is the excitation time corresponding to the $P \rightarrow M$ step, τ_{rel} is the relaxation time corresponding to the $M \rightarrow L$ step, A is a parameter related to the maximum of the energy curve, and the subscript i denotes the specific midrange mode considered. To keep the number of fitting parameters to a minimum, we fix the value of the excitation time at τ_{exc} = 0.73 ps, which is the relaxation time of the amide I mode to the first to third, sixth to eighth, and the group b_1 of INM$_t$'s. The energies of all of the intermediate modes are reasonably well fitted by eq 21, except for those of groups a_1 and a_2 for which we use the expression

$$E_i^{\mathrm{INM}_t}(t) - E_{i,\mathrm{eq}}^{\mathrm{INM}_t} = A(a_{\mathrm{rel}}e^{-t/\tau_{\mathrm{rel}}} + a'_{\mathrm{rel}}e^{-t/\tau'_{\mathrm{rel}}} - e^{-t/\tau_{\mathrm{exc}}}) \quad (22)$$

which contains two relaxation terms with times τ_{rel} and $\tau_{\mathrm{rel}}{}'$ and weights a_{rel} and $a_{\mathrm{rel}}{}'$ which satisfy $a_{\mathrm{rel}} + a_{\mathrm{rel}}{}' = 1$. The curves obtained from these fits are superimposed in Figures 4 and 5, and the values of the fit parameters obtained are included in Table 3. As observed, the fits nicely reproduce the results from the hybrid simulations. The fast relaxation times of the low-frequency modes, first to third INM$_t$'s, given in Table 3, are indicative of a fast energy transfer from these modes to the bath. In addition, the larger relaxation times obtained for modes sixth to eighth reveal that they are not strongly coupled to the solvent, as expected for low-frequency modes.

The excitation times of the mid- and high-frequency groups a_1 and a_2 included in Table 3 coincide with the amide I relaxation time of 0.73 ps. Moreover, the biexponential decays of these groups of modes reveal a first and fast relaxation step, with a common time of 2 ps, followed by a second and much slower relaxation step with rates close to that of the monoexponential decay of the group b_1 of modes. Interestingly, the weight of the first relaxation channel is higher for group a_1 than for group a_2, whereas for group a_2 the dominant relaxation channel is the second. We also observe in Table 3 that the slow excitation rates of the ninth (ν(CC)) and tenth (amide III) INM$_t$'s and group b_2 ($\nu(CH_3)$) of modes cannot be adjusted well by employing the amide I relaxation time but with larger τ_{exc} values. This confirms that these modes do not receive energy directly from the amide I but from the intermediate modes that participate in the first relaxation stage. The agreement between the τ_{exc} values of the ninth and tenth INM$_t$, and the τ_{rel} values of the groups a_1 and a_2 of modes seems to indicate that the energy transfers directly between them. Another possibility for the excitation of the ninth and tenth INM$_t$ is by receiving the energy released in the relaxation of the sixth to eighth INM$_t$s. Nevertheless, any attempt to fit the ninth and tenth INM$_t$ curves to faster excitation times gives poorer accuracy in the fits. We note also that the frequencies of the sixth to eighth INM$_t$ overlap nicely with the frequencies of the libration bands of liquid deuterated water,[139] indicating that the groups a_1 and a_2 of modes are better candidates to act as intermediates between amide I and the ninth and tenth INM$_t$s. Finally, the excitation time of 4.1 ps of the group b_2 of modes suggests that excitation of this group proceeds through secondary and quantitatively less important channels.

To sum up, our hybrid MDQT simulations results show that the VR of the amide I is essentially an IVR process, with a first relaxation step in which energy is transferred directly from the amide I mode to the group a_1 ($r(CH_3)$ + ν(CN)), the sixth (amide V) and eighth (amide VI) INM$_t$ and the low-frequency first-third INM$_t$'s, and a second minor relaxation channel which involves the participation of group a_2 ($\delta(CH_3)$) and the seventh (amide IV) INM$_t$'s. In the same time scale, a resonance-mediated energy transfer occurs from group a_2 to group b_1 ($\nu_s(CH_3)$), and the low-frequency modes then rapidly transfer their excess of vibrational energy to the solvent. In the second, and slower, IVR relaxation step, the energy flows from groups a_1 and a_2 to the ninth and tenth INM$_t$'s. Finally, medium- and high-frequency modes transfer the excess energy that remains in the solute molecule to the solvent in the final and slowest relaxation step.

For the sake of completeness, a comparison between the vibrational MDQT simulations carried out in this work and our previous classical simulations[68] is due. In Figure 6 we show the time-dependent vibrational energies of the intermediate modes that participate in the relaxation of the NMAD amide I mode in D_2O solution, extracted from both simulations. As previously reported,[68] the classical relaxation of the amide I mode takes place mainly through channels involving the seventh INM

dx.doi.org/10.1021/jp210727u | J. Phys. Chem. B 2012, 116, 2969−2980

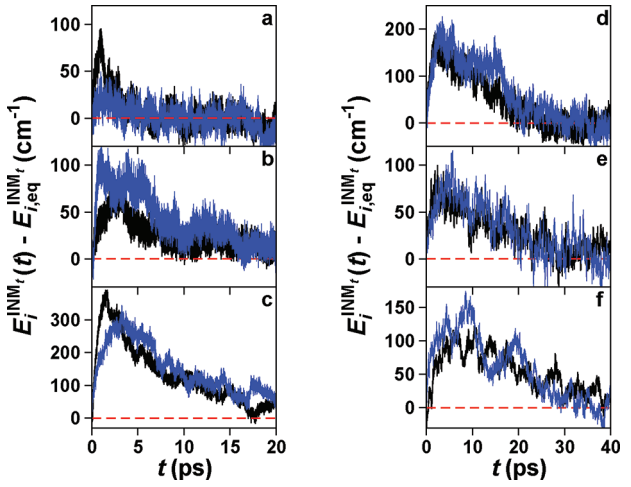

Figure 6. Time evolution of the vibrational energy of the (a) eighth INM_t, (b) tenth INM_t, (c) group a_1, (d) group a_2, (e) group b_1, and (f) group b_2 obtained from MDQT (black lines) and MD (blue lines) simulations.

(amide IV), the tenth INM (amide III), and the group a_1 ($r(CH_3)$ + ν(CN)) of modes. Classical and MDQT dynamics therefore agree in the identification of the modes of group a_1 as intermediate modes. The seventh and tenth INMs are replaced, however, by the sixth (amide V) and eighth (amide VI) INM_t's in the hybrid MDQT simulations as main intermediate modes, due to the decrease of the vibrational energy released by the amide I mode when going from the classical[68] (1692.7 cm^{-1}) to the MDQT (1464.7 cm^{-1}) simulations. This change of energy shifts the NMAD vibrational resonances from the seventh and tenth modes to the sixth and eighth modes, with a decrease in the vibrational frequencies[69] of 135 and 184 cm^{-1}, respectively.

The second major discrepancy between the classical and MDQT simulations concerns the role played by the low-frequency first-third INMs. As mentioned above, these modes receive large amounts of energy from the amide I mode (~300 cm^{-1}) at hops (see Table 2) and display similar fast excitations and subsequent fast relaxations. In contrast, no transient excess of energy is observed in the first to third modes in the classical simulations.[68] This discrepancy can be attributed to the larger classical amide I relaxation time, which prevents the accumulation of any excess of vibrational energy in these modes. Moreover, the negative or close to zero instantaneous frequencies commonly found for these modes make them quite difficult to analyze with other theoretical methods like time-dependent perturbation theory.[65,140,141] A recent energy flow analysis of the classical relaxation of the NMAD amide I mode in liquid D_2O[142] gave 350 cm^{-1} for the direct energy relaxation to the solvent, a value which is in rough agreement with the amount of energy directly transferred from the amide I to the low-frequency modes reported in Table 2.

The energy profiles of the midrange groups of modes a_1 and a_2 extracted from both classical and hybrid MDQT simulations are very similar, as observed in Figure 6c,d, with the hybrid description showing faster excitation times due to the faster hybrid amide I relaxation. Although there are differences in the maximum energy stored in these groups of modes, both simulations provide similar decays in which their equilibrium values are reached in the same time scale. As for the energy profiles of the high-frequency groups of modes b_1 and b_2 depicted in Figure 6e,f, both classical and hybrid simulations give a similar time evolution of the vibrational energy of these modes. It is also interesting to analyze the behavior of the 24th (amide A) INM. The excitation of this mode was reported to be fast in the classical MD simulations,[68] reaching a maximum content of energy of 80 cm^{-1}, in contrast with the slower and weaker excitation observed in the present vibrational MDQT simulations. This discrepancy arises from the fact that the flow of energy from the amide I mode to high-frequency modes is prevented during hops and that the amide A mode, which is the INM mode with the highest resemblance to the corresponding ENMs,[69] does not couple significantly with modes other than the amide I one.

Let us consider finally the time evolution of the total vibrational energy of the NMAD molecule. Recent ultrafast time-resolved infrared-Raman spectroscopic measurements[55] reported a relaxation time for this process of 5.1 ps. Although this value was obtained after excitation of the NMAD C−H stretching modes ($\nu_s(CH_3)$), no significant differences are expected after excitation of the amide I mode. On the other hand, previous classical nonequilibrium MD simulations of the VR of either the $\nu_s(CH_3)$ mode or the amide I mode[68,69] gave a relaxation time close to 10 ps for the decay of the total vibrational energy of the NMAD molecule in D_2O solution. In Figure 7 we show now the total vibrational energy of the

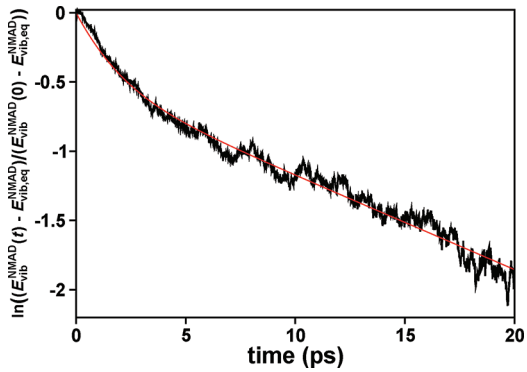

Figure 7. Normalized time evolution of the vibrational energy of the NMAD molecule in liquid D_2O with respect to its equilibrium value (logarithmic scale), with the adjustment curves to the biexponential functions superimposed (red line).

NMAD molecule as a function of time extracted from the hybrid MDQT simulations. This energy flow can be fitted well to the biexponential function

$$\frac{E_{vib}^{NMAD}(t) - E_{vib,eq}^{NMAD}}{E_{vib}^{NMAD}(0) - E_{vib,eq}^{NMAD}} = c_1 e^{-t/\tau_{rel,1}} + c_2 e^{-t/\tau_{rel,2}} \quad (23)$$

where c_1 and c_2 are the exponential amplitudes satisfying $c_1 + c_2 = 1$, and $\tau_{rel,1}$, and $\tau_{rel,2}$ are the relaxation times thereof. Two well-separated relaxation times are then obtained, with values $\tau_{rel,1}$ = 1.53 ps (39%) and $\tau_{rel,2}$ = 14.7 ps (61%), from which we can infer that the whole relaxation process takes place in two well-defined stages with different relaxation mechanisms. The first relaxation time $\tau_{rel,1}$ accounts for the relaxation of the lowest frequency vibrations (first to third and sixth to eighth INM_t's), which occur faster due to their strong couplings with the bath. The weight of this relaxation channel also indicates that ≈40% of the total vibrational energy is funnelled through this mechanism, an amount which is quite close to the percentage

dx.doi.org/10.1021/jp210727u | J. Phys. Chem. B 2012, 116, 2969−2980

of energy transferred from the amide I to the low frequency modes (see Table 2). The second relaxation time, $\tau_{rel,2}$, lies in the same time scale as that of both the relaxation times of the high-frequency group of modes b_1 and b_2 and the relaxation time of the groups a_1 and a_2 of modes in the second relaxation stage. To make a proper comparison of the MDQT biexponential decay with the previous experimental[55] and classical[68,69] monoexponential decays, we employ the time at which the initial vibrational energy decays by a factor of $1/e$. Thus we obtain a relaxation time of 6.6 ps, which is closer to the experimental values than that extracted from the classical MD simulations. The decrease of the NMAD relaxation time obtained from the vibrational MDQT simulations, as compared with that from the classical simulations, is due to the faster relaxation time achieved by the amide I mode. Furthermore, the quantum release of the energy stored in the amide I mode may lead to larger perturbations of the intermediate modes than those brought about by the continuous relaxation of this mode during the classical simulations. Larger geometrical distortions are therefore expected from the hybrid simulations which may result in an increase of the couplings between the intermediate modes and the subsequent decrease of the whole VR time.

4. CONCLUSIONS

In this work we have carried out nonequilibrium hybrid quantum-classical MD simulations of the VR of the NMAD amide I mode in D_2O solution. A novel implementation of the vibrational MDQT method has been developed which deals explicitly with the quantum mechanical treatment of one normal mode of the solute polyatomic molecule and the conventional classical treatment of the remaining degrees of freedom. INMs of the NMAD defined at initial time $t = 0$ (INM_0) are shown to be suitable coordinates to conduct the hybrid simulations since they achieve the best compromise between a proper initial definition of the quantum and classical subsystems and an accurate hybrid quantum/classical propagation during the VR. The ultimate evaluation of the time evolution of the energy stored in each individual normal mode is made by using the hybrid INMs (INM_t). Both the INM_0's and the hybrid INM_t are identified and assigned using the ENMs as templates.

The results obtained from the hybrid MDQT simulations show that inclusion of quantum effects in nonequilibrium MD notably modifies the dynamics of the VR of the amide I mode, which turns out to be significantly faster than that from previous classical simulations, and also in better agreement with experiments. Furthermore, the hybrid MDQT simulations reveal different aspects of the VR of the individual quantum normal mode within a classical polyatomic molecule that should be taken into account in future vibrational MDQT descriptions. First, the time evolution of quantum populations of the initial excited mode may show nonphysical short-time oscillations not directly related to the global relaxation process. These oscillations may lead to an unsuitable ultrafast divergence between the average quantum and classical populations, which can be amended by evaluation of the quantum transitions only after every period of them, thus obtaining significant improvements in the expected match between classical and quantum populations during the very first stage of the relaxation process. Second, the nonphysical energy transfer that occurs to high-frequency normal modes, previously reported in several nonequilibrium classical MD simulations, can be avoided by preventing the energy flow to these modes during the hybrid hops, without altering the distribution of the energy transferred to the low- and mid-frequency modes. Finally, the direct intra- and intermolecular energies released by the initially excited quantum amide I mode can be calculated separately from the energy redistribution at the hops. This information turns out to be very useful in discerning the origin of the excitation of several intermediate normal modes during the VR of the whole molecule.

The hybrid MDQT simulations carried out in this work confirm that the relaxation of the amide I mode is essentially an intramolecular vibrational redistribution process, in agreement with previous theoretical and experimental studies, with little contribution from the solvent molecules. We have identified and described the specific hybrid IVR relaxation pathways that follows the relaxation of the amide I mode and compared them with the results from previous classical MD simulations. Thus we have discerned the role played by the low-frequency modes acting as intermediate modes between the amide I and the solvent. This fast and highly efficient energy relaxation channel could not be detected in classical simulations. In addition, it has been shown that the mid-range and high-frequency modes behave quite similarly, with some slight differences between them arising from the faster transfer of the energy released by the amide I mode and the resonance shift caused by the hybrid nature of this mode.

The discrete quantum energy transfer from the hybrid amide I mode to the rest of the NMAD molecule accelerates the whole VR process, in which two different well-defined relaxation mechanisms are identified. The faster mechanism accounts for ≈40% of the total vibrational energy and takes place with the participation of the lowest frequency vibrations as short-life intermediate modes. The second and slower mechanism accounts for the remaining ≈60% of the energy, which is funnelled through specific mid-range and high-frequency modes.

The vibrational MDQT implementation presented in this work can be considered as a first step in the development of new nonequilibrium hybrid quantum/classical approaches designed to simulate the VR of real polyatomic molecules, like peptides, in liquids. This theoretical formulation runs parallel and on the same track with the most recent advances in time-resolved infrared-Raman spectroscopic measurements and can be straightforwardly extended to treat more than one degree of freedom quantum-mechanically.

AUTHOR INFORMATION

Corresponding Author

*E-mail: bastida@um.es; sfalberti@gmail.com.

Notes

The authors declare no competing financial interest.

ACKNOWLEDGMENTS

This work was partially supported by the Ministerio de Ciencia e Innovación of Spain under Project CTQ2011-25872 and CONSOLIDER CSD2009-00038 and by the Fundación Séneca del Centro de Coordinación de la Investigación de la Región de Murcia under Project 08735/PI/08, by the Universidad Nacional de Quilmes, and by CONICET. A.K. acknowledges a fellowship provided by CONICET.

REFERENCES

(1) Laubereau, A.; Kaiser, W. *Rev. Mod. Phys.* **1978**, 607.
(2) Miller, R. J. D. *Annu. Rev. Phys. Chem.* **1991**, *42*, 581.

(3) Mizutani, Y.; Kitagawa, T. *Science* **1997**, *278*, 443.
(4) Hamm, P.; Lim, M. H.; Hochstrasser, R. M. *J. Phys. Chem. B* **1998**, *102*, 6123−6138.
(5) Dlott, D. D. *Chem. Phys.* **2001**, *266*, 149.
(6) Zanni, M. T.; Asplund, M. C.; Hochstrasser, R. M. *J. Chem. Phys.* **2001**, *114*, 4579−4590.
(7) Fayer, M. D. *Annu. Rev. Phys. Chem.* **2001**, *52*, 315.
(8) Woutersen, S.; Hamm, P. *J. Phys.: Condens. Matter* **2002**, *14*, R1035.
(9) Nagy, A. M.; Prokhorenko, V. I.; Miller, R. J. D. *Curr. Opin. Struct. Biol.* **2006**, *16*, 654.
(10) DeFlores, L. P.; Ganim, Z.; Ackley, S. F.; Chung, H. S.; Tokmakoff, A. *J. Phys. Chem. B* **2006**, *110*, 18973−18980.
(11) Wang, Z.; Carter, J. A.; Lagutchev, A.; Koh, Y. K.; Seong, N.-H.; Cahill, D. G.; Dlott, D. D. *Science* **2007**, *317*, 787.
(12) Hamm, P.; Helbing, J.; Bredenbeck, J. *Annu. Rev. Phys. Chem.* **2008**, *59*, 291−317.
(13) Fayer, M. D. *Annu. Rev. Phys. Chem.* **2009**, *60*, 21−38.
(14) Mukamel, S.; Hochstrasser, R. M. *Chem. Phys.* **2001**, *266*, 135−351.
(15) Oxtoby, D. W. *Adv. Chem. Phys.* **1981**, *47*, 487−519.
(16) Rey, R.; Moller, K. B.; Hynes, J. T. *Chem. Rev.* **2004**, *104*, 1915.
(17) Lawrence, C. P.; Skinner, J. L. *J. Chem. Phys.* **2002**, *117*, 5827.
(18) Lawrence, C. P.; Skinner, J. L. *J. Chem. Phys.* **2002**, *117*, 8847.
(19) Lawrence, C. P.; Skinner, J. L. *J. Chem. Phys.* **2003**, *118*, 264.
(20) Piryatinski, A.; Lawrence, C. P.; Skinner, J. L. *J. Chem. Phys.* **2003**, *118*, 9664.
(21) Shiga, M.; Okazaki, S. *J. Chem. Phys.* **1999**, *111*, 5390.
(22) Okazaki, S. *Adv. Chem. Phys.* **2001**, *118*, 191−270.
(23) Terashima, T.; Shiga, M.; Okazaki, S. *J. Chem. Phys.* **2001**, *114*, 5663−5673.
(24) Sato, M.; Okazaki, S. *J. Chem. Phys.* **2005**, *123*, 124508.
(25) Sato, M.; Okazaki, S. *J. Mol. Liq.* **2005**, *119*, 15−22.
(26) Navrotskaya, I.; Geva, E. *J. Phys. Chem. A* **2007**, *111*, 460.
(27) Navrotskaya, I.; Geva, E. *J. Chem. Phys.* **2007**, *127*, 054504.
(28) Leitner, D. M.; Levine, B.; Quenneville, J.; Martínez, T. J.; Wolynes, P. G. *J. Phys. Chem. A* **2003**, *107*, 10706−10716.
(29) Leitner, D. M. *Adv. Chem. Phys.* **2005**, *130(B)*, 205−206.
(30) Leitner, D. M.; Gruebele, M. *Mol. Phys.* **2008**, *106*, 433−442.
(31) Fujisaki, H.; Zhang, Y.; Straub, J. Non-Markovian Theory of Vibrational Energy Relaxation and its Applications to Biomolecular Systems. In *Advancing Theory for Kinetics and Dynamics of Complex, Many-Dimensional Systems: Clusters and Proteins*; Advances in Chemical Physics, Volume *145*; Wiley: New York, 2011.
(32) Sagnella, D. E.; Straub, J. E. *Biophys. J.* **1999**, *77*, 70.
(33) Bu, L.; Straub, J. E. *Biophys. J.* **2003**, *85*, 1429.
(34) Yu, X.; Leitner, D. M. *J. Phys. Chem. B* **2003**, *107*, 1698−1707.
(35) Yu, X.; Leitner, D. M. *J. Chem. Phys.* **2005**, *122*, 054902.
(36) Sharp, K.; Skinner, J. J. *Proteins* **2006**, *65*, 347−361.
(37) Leitner, D. M. *Annu. Rev. Phys. Chem.* **2008**, *59*, 233−259.
(38) Leitner, D. M. *J. Chem. Phys.* **2009**, *130*, 195101.
(39) Leitner, D. M.; Straub, J. E. *Proteins: Energy, Heat and Signal Flow (Computation in Chemistry)*; Taylor and Francis: London, 2009.
(40) Leitner, D. M. *New J. Phys.* **2010**, *12*, 085004.
(41) Botan, V.; Backus, E. H. G.; Pfister, R.; Moretto, A.; Crisma, M.; Toniolo, C.; Nguyen, P. H.; Stock, G.; Hamm, P. *Proc. Natl. Acad. Sci. U.S.A.* **2007**, *104*, 12749−12754.
(42) Backus, E. H. G.; Nguyen, P. H.; Botan, V.; Pfister, R.; Moretto, A.; Crisma, M.; Toniolo, C.; Stock, G.; Hamm, P. *J. Phys. Chem. B* **2008**, *112*, 9091−9099.
(43) Backus, E. H. G.; Nguyen, P. H.; Botan, V.; Moretto, A.; Crisma, M.; Toniolo, C.; Zerbe, O.; Stock, G.; Hamm, P. *J. Phys. Chem. B* **2008**, *112*, 15487−15492.
(44) Backus, E. H. G.; Bloem, R.; Pfister, R.; Moretto, A.; Crisma, M.; Toniolo, C.; Hamm, P. *J. Phys. Chem. B* **2009**, *113*, 13405−13409.
(45) Krimm, S.; Bandekar, J. *Adv. Protein Chem.* **1986**, *38*, 181.
(46) Moran, A.; Mukamel, S. *J. Chem. Phys.* **2003**, *118*, 9971.
(47) Moran, A.; Mukamel, S. *Proc. Natl. Acad. Sci.* **2004**, *101*, 506−510.
(48) Peterson, K. A.; Rella, C. W.; Engholm, J. R.; Schwettman, H. A. *J. Phys. Chem. B* **1999**, *103*, 557−561.
(49) Xie, A.; van der Meer, L.; Hoff, W.; Austin, R. *Phys. Rev. Lett.* **2000**, *84*, 5435.
(50) Austin, R.; Xie, A.; van der Meer, L.; Redlich, B.; Lindgard, P.; Frauenfelder, H.; Fu., D. *Phys. Rev. Lett.* **2005**, *94*, 128101.
(51) Woutersen, S.; Mu, Y.; Stock, G.; Hamm, P. *Proc. Natl. Acad. Sci. U.S.A.* **2001**, *98*, 11254.
(52) Woutersen, S.; Pfister, R.; Hamm, P.; Mu, Y. G.; Kosov, D. S.; Stock, G. *J. Chem. Phys.* **2002**, *117*, 6833−6840.
(53) Rubtsov, I. V.; Wang, J.; Hochstrasser, R. M. *J. Phys. Chem. A* **2003**, *107*, 3384−3396.
(54) DeCamp, M. F.; DeFlores, L.; McCracken, J. M.; Tokmakoff, A.; Kwac, K.; Cho, M. *J. Phys. Chem. B* **2005**, *109*, 11016−11026.
(55) Fang, Y.; Shigeto, S.; Seong, N.; Dlott, D. *J. Phys. Chem. A* **2009**, *113*, 75−84.
(56) Piatkowski, L.; Bakker, H. J. *J. Phys. Chem. A* **2010**, *114*, 11462−11470.
(57) Gregurick, S. K.; Chaban, G. M.; Gerber, R. B. *J. Phys. Chem. A* **2002**, *106*, 8696−8707.
(58) Nguyen, P. H.; Stock, G. *J. Chem. Phys.* **2003**, *119*, 11350−11358.
(59) Kwac, K.; Cho, M. H. *J. Chem. Phys.* **2003**, *119*, 2247−2255.
(60) Schmidt, J. R.; Corcelli, S. A.; Skinner, J. L. *J. Chem. Phys.* **2004**, *121*, 8887−8896.
(61) Hayashi, T.; Zhuang, W.; Mukamel, S. *J. Phys. Chem. A* **2005**, *109*, 9747−9759.
(62) Fujisaki, H.; Zhang, Y.; Straub, J. E. *J. Chem. Phys.* **2006**, *124*, 144910.
(63) Dijkstra, A. G.; Jansen, T. C.; Bloem, R.; Knoester, J. *J. Chem. Phys.* **2007**, *127*, 194505.
(64) Fujisaki, H.; Yagi, K.; Hirao, K.; Straub, J. E. *Chem. Phys. Lett.* **2007**, *443*, 6−11.
(65) Fujisaki, H.; Stock, G. *J. Chem. Phys.* **2008**, *129*, 134110.
(66) Park, S.; Nguyen, P. H.; Stock, G. *J. Chem. Phys.* **2010**, *131*, 184503.
(67) Fujisaki, H.; Yagi, K.; Straub, J. E.; Stock, G. *Int. J. Quantum Chem.* **2009**, *109*, 2047−2057.
(68) Bastida, A.; Soler, M. A.; Zúñiga, J.; Requena, A.; Kalstein, A.; Fernández-Alberti, S. *J. Chem. Phys.* **2010**, *132*, 224501.
(69) Bastida, A.; Soler, M. A.; Zúñiga, J.; Requena, A.; Kalstein, A.; Fernández-Alberti, S. *J. Phys. Chem. A* **2010**, *114*, 11450−11461.
(70) Goodyear, G.; Stratt, R. M. *J. Chem. Phys.* **1997**, *107*, 3098.
(71) David, E. F.; Stratt, R. M. *J. Chem. Phys.* **1998**, *109*, 1375−1390.
(72) Cho, M.; Fleming, G. R.; Saito, S.; Ohmine, I.; Stratt, R. M. *J. Chem. Phys.* **1994**, *100*, 6672.
(73) Ladany, B. M.; Klein, S. *J. Chem. Phys.* **1996**, *105*, 1552.
(74) Stratt, R. M.; Cho, M. *J. Chem. Phys.* **1994**, *100*, 6700.
(75) Keyes, T. *J. Phys. Chem. A* **1997**, *101*, 2921−2930.
(76) Ladany, B. M.; Stratt, R. M. *J. Phys. Chem.* **1995**, *99*, 2502.
(77) Ladany, B. M.; Stratt, R. M. *J. Phys. Chem.* **1996**, *100*, 1266.
(78) Kalstein, A.; Fernández-Alberti, S.; Bastida, A.; Soler, M. A.; Farag, M. H.; Zúñiga, J.; Requena, A. *Theor. Chem. Acc.* **2011**, *128*, 769−782.
(79) Rey, R.; Hynes, J. T. *J. Chem. Phys.* **1998**, *108*, 142−153.
(80) Li, S.; Thompson, W. H. *Chem. Phys. Lett.* **2005**, *405*, 304.
(81) Zhang, Y.; Fujisaki, H.; Straub, J. E. *J. Phys. Chem. A* **2009**, *113*, 3051−3060.
(82) Coker, D. F.; Mei, H. S.; Ryckaert, J.-P. Thermal average time correlation functions from non-adiabatic MD: application to rate constants for a condensed phase non-adiabatic reactions. In *Classical and Quantum Dynamics in Condensed Phase Simulations*; Berne, B. J., Ciccotti, G., Coker, D. F., Eds.; World Scientific: Singapore, 1998; p 539.
(83) Rossky, P. J. Non-adiabatic Quantum Dynamics Simulation Using Classical Baths. In *Classical and Quantum Dynamics in Condensed Phase Simulations*; Berne, B. J., Ciccotti, G., Coker, D. F., Eds.; World Scientific: Singapore, 1998; p 515.

(84) Tully, J. C. Mixed quantum-classical dynamics: mean-field and surface hopping. In *Classical and Quantum Dynamics in Condensed Phase Simulations*; Berne, B. J., Ciccotti, G., Coker, D. F., Eds.; World Scientific: Singapore, 1998; p 489.
(85) Pierdominici-Sottile, G.; Fernandez-Alberti, S.; Palma, J. *Adv. Quantum Chem.* **2010**, *59*, 247.
(86) Tully, J. C.; Preston, R. K. *J. Chem. Phys.* **1971**, *55*, 562.
(87) Tully, J. C. *J. Chem. Phys.* **1990**, *93*, 1061−1071.
(88) Tully, J. C. Nonadiabatic dynamics. In *Modern methods for multidimensional dynamics computations in chemistry*; Thompson, D. L., Ed.; World Scientific: Singapore, 1998; pp 34−72.
(89) Tully, J. C. *Faraday Discuss.* **1998**, *110*, 1−13.
(90) McLachlan, A. *Mol. Phys.* **1964**, *8*, 39−44.
(91) Billing, G. *Int. Rev. Phys. Chem.* **1994**, *13*, 309−335.
(92) Makri, N. *Annu. Rev. Phys. Chem.* **1999**, *50*, 167−191.
(93) Hack, M. D.; Thrular, D. G. *J. Phys. Chem. A* **2000**, *104*, 7917−7926.
(94) Kohen, D.; Stillinger, F. H.; Tully, J. C. *J. Chem. Phys.* **1998**, *109*, 4713.
(95) Hanna, G.; Geva, E. *J. Phys. Chem. B* **2008**, *112*, 4048−4058.
(96) Hanna, G.; Geva, E. *J. Phys. Chem. B* **2008**, *112*, 15793−15800.
(97) Hanna, G.; Geva, E. *J. Phys. Chem. B* **2009**, *113*, 9278−9288.
(98) Hanna, G.; Geva, E. *J. Phys. Chem. B* **2011**, *115*, 5191−5200.
(99) Bastida, A.; Zúñiga, J.; Requena, A.; Halberstadt, N.; Beswick, J. A. *J. Chem. Phys.* **1998**, *109*, 6320.
(100) Bastida, A.; Zúñiga, J.; Requena, A.; Halberstadt, N.; Beswick, J. A. *Chem. Phys.* **1999**, *240*, 229−239.
(101) Bastida, A.; Miguel, B.; Zúñiga, J.; Requena, A.; Halberstadt, N.; Janda, K. C. *J. Chem. Phys.* **1999**, *111*, 4577.
(102) Fernandez-Alberti, S.; Halberstadt, N.; Beswick, J. A.; Bastida, A.; Zúñiga, J.; Requena, A. *J. Chem. Phys.* **1999**, *111*, 239.
(103) Miguel, B.; Bastida, A.; Zúñiga, J.; Requena, A.; Halberstadt, N. *J. Chem. Phys.* **2000**, *113*, 10130.
(104) Bastida, A.; Miguel, B.; Zúñiga, J.; Requena, A.; Halberstadt, N. *Faraday Discuss.* **2001**, *118*, 257.
(105) Hammes-Schiffer, S.; Tully, J. C. *J. Chem. Phys.* **1994**, *101*, 4657−4667.
(106) Li, S.; Thompson, W. H. *J. Phys. Chem. A* **2003**, *107*, 8696−8704.
(107) Thompson, W. H. *J. Chem. Phys.* **2003**, *118*, 1059−1067.
(108) Fernandez-Alberti, S.; Echave, J.; Engel, V.; Halberstadt, N.; Beswick, J. A. *J. Chem. Phys.* **2000**, *113*, 1027.
(109) Bastida, A.; Cruz, C.; Zúñiga, J.; Requena, A.; Miguel, B. *J. Chem. Phys.* **2004**, *121*, 10611−10622.
(110) Herman, M. F. *J. Chem. Phys.* **1987**, *87*, 4794.
(111) Bastida, A.; Cruz, C.; Zúñiga, J.; Requena, A.; Miguel, B. *Chem. Phys. Lett.* **2006**, *417*, 53.
(112) Bastida, A.; Zúñiga, J.; Requena, A.; Miguel, B. *J. Chem. Phys.* **2008**, *129*, 154501−154510.
(113) Bastida, A.; Zúñiga, J.; Requena, A.; Miguel, B. *J. Chem. Phys.* **2009**, *131*, 204505−204514.
(114) Fang, J.; Hammes-Schiffer, S. *J. Phys. Chem. A* **1999**, *103*, 9399−9407.
(115) Fang, J.; Hammes-Schiffer, S. *J. Chem. Phys.* **1999**, *110*, 11166−11175.
(116) Nakamura, M.; Tamura, K.; Murakami, S. *Thermochim. Acta* **1995**, *253*, 127−136.
(117) Cornell, W. D.; Cieplak, P.; Bayly, C. I.; Gould, I. R.; Merz, K. M.; Ferguson, D. M.; Spellmeyer, D. C.; Fox, T.; Caldwell, J. W.; Kollman, P. A. *J. Am. Chem. Soc.* **1995**, *117*, 5179−5197.
(118) MacKerell, A. D. Jr.; Bashford, D.; Bellott, M.; Dunbrack, R. L. Jr.; Evanseck, J. D.; Field, M. J.; Fischer, S.; Gao, J.; Guo, H.; Ha, S.; et al. *J. Phys. Chem. B* **1998**, *102*, 3586−3616.
(119) Pappu, R. V.; Hart, R. K.; Ponder, J. W. *J. Phys. Chem. B* **1998**, *102*, 9725−9742.
(120) Allen, M. P.; Tildesley, D. J. *Computer simulation of liquids*; Oxford Science Publications: Oxford, 1987.
(121) Svanberg, M. *Mol. Phys.* **1997**, *92*, 1085−1088.
(122) Bastida, A.; Soler, M. A.; Zúñiga, J.; Requena, A.; Miguel, B. *Chem. Phys.* **2009**, *358*, 57−60.
(123) Berendsen, H. J. C.; Postma, J. P. M.; Gunsteren, W. F. V.; DiNola, A.; Haak, J. R. *J. Chem. Phys.* **1984**, *81*, 3684−3690.
(124) Mauri, F.; Car, R.; Tosatti, E. *Europhys. Lett.* **1993**, *24*, 431−436.
(125) Müller, U.; Stock, G. *J. Chem. Phys.* **1997**, *107*, 6230−6245.
(126) Käb, G. *Phys. Rev. E* **2002**, *66*, 046117.
(127) Neufeld, A.; Schwarzer, D.; Schroeder, J.; Troe, J. *J. Chem. Phys.* **2003**, *119*, 2502−2512.
(128) Käb, G. *J. Phys. Chem. A* **2004**, *108*, 8866−8877.
(129) Parandekar, P. V.; Tully, J. C. *J. Chem. Phys.* **2005**, *122*, 094102.
(130) Käb, G. *J. Phys. Chem. A* **2006**, *110*, 3197−3215.
(131) Parandekar, P. V.; Tully, J. C. *J. Chem. Theory Comput.* **2006**, *2*, 229−235.
(132) Bastida, A.; Cruz, C.; Zúñiga, J.; Requena, A.; Miguel, B. *J. Chem. Phys.* **2007**, *126*, 014503.
(133) Stock, G. *Phys. Rev. Lett.* **2009**, *102*, 118301.
(134) Déak, J. C.; Iwaki, L. K.; Dlott, D. D. *J. Phys. Chem. A* **1998**, *102*, 8193−8201.
(135) Déak, J. C.; Iwaki, L. K.; Dlott, D. D. *J. Phys. Chem. A* **1999**, *103*, 971−979.
(136) Déak, J. C.; Iwaki, L. K.; Dlott, D. D. *J. Raman Spectrosc.* **2000**, *31*, 263−274.
(137) Alfano, R. R.; Shapiro, S. L. *Phys. Rev. Lett.* **1972**, *29*, 1655−1658.
(138) Seilmeier, A.; Kaiser, W. Ultrashort intramolecular and intermolecular vibrational energy transfer of polyatomic molecules in liquids. In *Ultrashort laser pulses and applications*; Kaiser, W., Ed.; Springer-Verlag: Berlin, 1988; Vol. *60*, p 279.
(139) Zelsmann, H. R. *J. Mol. Struct.* **1995**, *350*, 95−114.
(140) Moritsugu, K.; Miyashita, O.; Kidera, A. *Phys. Rev. Lett.* **2000**, *85*, 3970−3973.
(141) Moritsugu, K.; Miyashita, O.; Kidera, A. *J. Phys. Chem. B* **2003**, *107*, 3309−3317.
(142) Soler, M.; Bastida, A.; Farag, M. H.; Zúñiga, J.; Requena, A. *J. Chem. Phys.* **2011**, *135*, 204106.